www.sciencedirect.com
Corrosion Science 49 (2007) 139–148
www.elsevier.com/locate/corsci

Doi:10.1016/j.corsci.2006.05.013

In-situ observation of intergranular stress corrosion cracking in AA2024-T3 under constant load conditions

Xiaodong Liu [a], G.S. Frankel [a,*], B. Zoofan [b], S.I. Rokhlin [b]

[a] Fontana Corrosion Center, Department of Materials Science and Engineering, The Ohio State University, Columbus, OH 43210, USA
[b] Department of Industrial, Welding and Systems Engineering, The Ohio State University, Columbus, OH 43210, USA

Abstract

A specially designed setup was used to apply a constant load to a thin sheet sample of AA2024-T3 and, using microfocal X-ray radiography, to observe in situ the resulting intergranular stress corrosion cracking (IGSCC) from the exposed edge of the sample. The growth of and competition between multiple IGSCC sites was monitored. In many experiments twin cracks initiated close to each other. Furthermore, the deepest crack at the beginning of every experiment was found to slow or stop growing, and was then surpassed by another crack that eventually penetrated through the sample. These observations cannot be explained by the theory of fracture mechanics in inert environments. The possible mechanisms underlying the competition between cracks are discussed.

1. Introduction

The pronounced susceptibility of high strength aluminum alloys to intergranular stress corrosion cracking (IGSCC) seriously limits their lifetime as engineering materials [1]. The propagation kinetics of cracks along the grain boundaries (GBs) [2,3], and interaction between the microstructure and local environment [4] have been studied. Anodic dissolution associated with precipitates along GBs is considered to be the primary mechanism of stress corrosion cracking (SCC) in high strength 2xxx (Al–Cu–Mg) series alloys [5,6]. Galvanic interaction between the particles and the local surrounding matrix can lead to preferential dissolution of anodic particles or dissolution of the adjacent matrix surrounding noble particles [7–10]. Evolution of hydrogen always occurs in actively growing localized corrosion sites and cracks· The absorption of hydrogen into the aluminum alloy leads to the possibility of crack propagation by hydrogen embrittlement (HE) [11,12].

Conventionally, investigations of SCC growth have been performed using configurations such as the double cantilever beam (DCB), the constraints of which allow only a single crack per specimen [3]. In contrast, multiple intergranular corrosion (IGC) cracks exist in real structures. The stress intensity for periodically spaced edge cracks in a semi-infinite body has been addressed [13,14]. However, the situation for multiple cracks of varying length and spacing is still unclear. In recent studies, we have described the use of X-ray radiography to image in situ the initiation and growth of multiple IGC sites in AA2024 using a modified ASTM-G49 stressing jig to apply a fixed displacement [15–17]. Competition between multiple IGCs was observed. In this study, X-ray microfocal radiography was put to further use in the study of IGSCC in AA2024-T3 with a setup that applied constant load rather than constant elongation, thereby allowing calculation of the stress intensity at the crack tips.

2. Experimental

Sheet samples were cut from a wrought AA2024-T3 plate (Cu 4.5%, Mg 1.45%, Mn 0.57%, Si 0.11%, Fe 0.25%, Zn 0.09%, Ti 0.02%, Cr 0.01%, and other elements total 0.05% max) with 19 mm thickness. Details of the experimental procedure are given elsewhere [18]. The samples had dimensions of 80 mm in the S (short transverse) direction × 4 mm in the L (longitudinal or rolling) direction, and were reduced in thickness along the T (transverse) direction to 1.05 mm by grinding and polishing. The sample was stressed in the S direction and a part of the L face of the sample (12 × 1.05 mm) was exposed to 1.0 M NaCl solution, allowing cracking in the L direction. Tabs of the same material were laser-welded in the S direction to plate sections to extend their length [19].

A constant load was applied along the sample length using a specially designed constant load fixture that gripped the sample on both ends, Fig. 1. One set of grips was stationary and bolted into the base plate. The other set contained nylon wheels sliding along the base plate. A stainless steel cable connected the movable grips over a stationary pulley to hanging weights to create the constant load. As the cracks extended, the sample deformation was accommodated by motion of the movable grips, which maintained a constant load.

The X-ray microfocal radiographic imaging technique was performed using a 225-kV, 3-mA X-ray source with 3–5 μm focal size and a positioning system with 2 μm linear resolution. To obtain optimum resolution for a 1.05 mm thick Al alloy sample, a 40 kV source voltage and 200 μA current were used. The X-rays irradiated the T face of the sample and then illuminated special film, as described previously [19,20]. Absorption of the X-rays by the sample resulted in a negative, gray-scale, radiographic image, in which higher density regions such as intermetallic particles were bright and lower density regions associated with intergranular sites or corrosion product were dark. The same electrochemical cell used in the fixed displacement experiments and described in detail elsewhere [15] was sealed on the top of samples, allowing potentiostatic polarization at —580 mV SCE in 1.0 M NaCl by the potentiostat system.

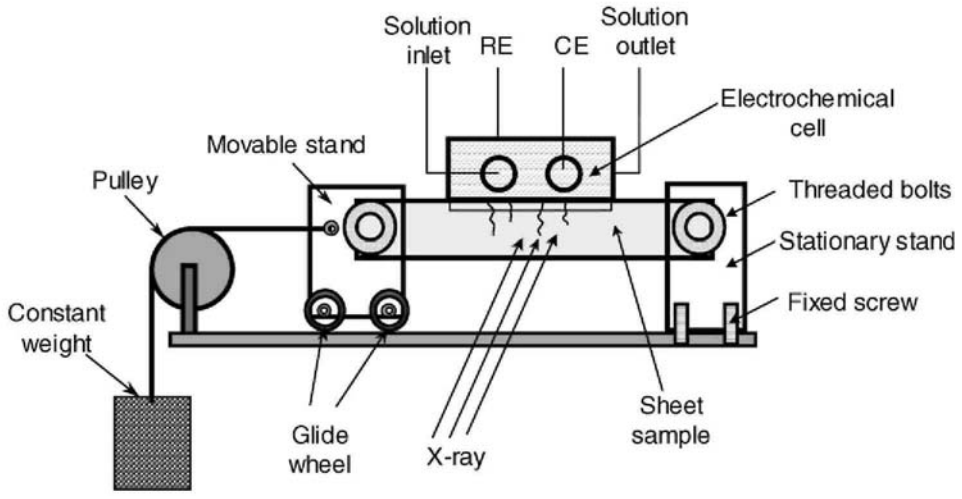

Fig. 1. Schematic drawing of fixture used to apply a uniaxial constant load.

3. Results

3.1. In situ radiography evaluation

A constant load resulting in an initial stress of 77 MPa (23% of the yield stress) was applied [19]. Fig. 2 shows radiographic images of the L–S sample during the experiment. The top edge of each image was the sample surface exposed to solution. The vertical white streaks in Fig. 2(a) are associated with intermetallic particles aligned in the L direction. The horizontal white line 1.5 mm below the top surface resulted from the red lacquer sealing the edge of the cell lips, as described in detail elsewhere [15,16]. The cracks show up as thick, dark vertical lines initiating at the top exposed surface and growing downwards in the L direction. X-ray radiography is an integration of the microstructure rather than a reflection of continuous microstructure.

As shown in Fig. 2, sharp cracks protrude downwards from some of the sites across the sample. A crack marked at site 1 in Fig. 2(a) formed first, and another crack at site 2 was found later after 20 min. Prior to 30 min, Fig. 2(b), these two cracks were similar in length, although crack 2 appeared to be darker and wider. After 1 h, Fig. 2(c), a twin crack at site 3 became evident and was deeper than the cracks at the other sites. After 1.75 h, the twin cracks at site 3 were more clearly seen to be the deepest in the sample (Fig. 2(d)). Close examination of Fig. 2(d) reveals some shallow cracks initiated at site 4, just to the right of site 2, which eventually became the failure crack as described below. Fig. 2(e) and (f), after 3 and 6.5 h, respectively, show that the cracks at sites 1 and 2 stopped growing. The cracks at site 3 continued to be the clearest and deepest in the sample, but there was no evident crack growth there either. After 6.5 h, however, the cracks at site 4 advanced rapidly. During the 30 min period between Fig. 2(f) and (g), the nominal growth rate of the large crack at site 4 was approximately 0.06 mm/min, and this crack penetrated through the sample shortly afterwards. Fig. 2(h) shows the broken sample that was unloaded and removed from the cell. Besides the failure crack, the long stifled cracks and short IGC sites are evident.

The crack-stopping phenomenon was reproducible. Other experiments were performed at different loading levels and in each one, the deepest crack at the beginning of the experiment stifled and was later passed by another crack [18]. Stifling of initial long cracks was also observed in our recent work with a fixed displacement stressing jig [15,16]. Determination of stress intensity is facilitated by the constant load setup as discussed presently.

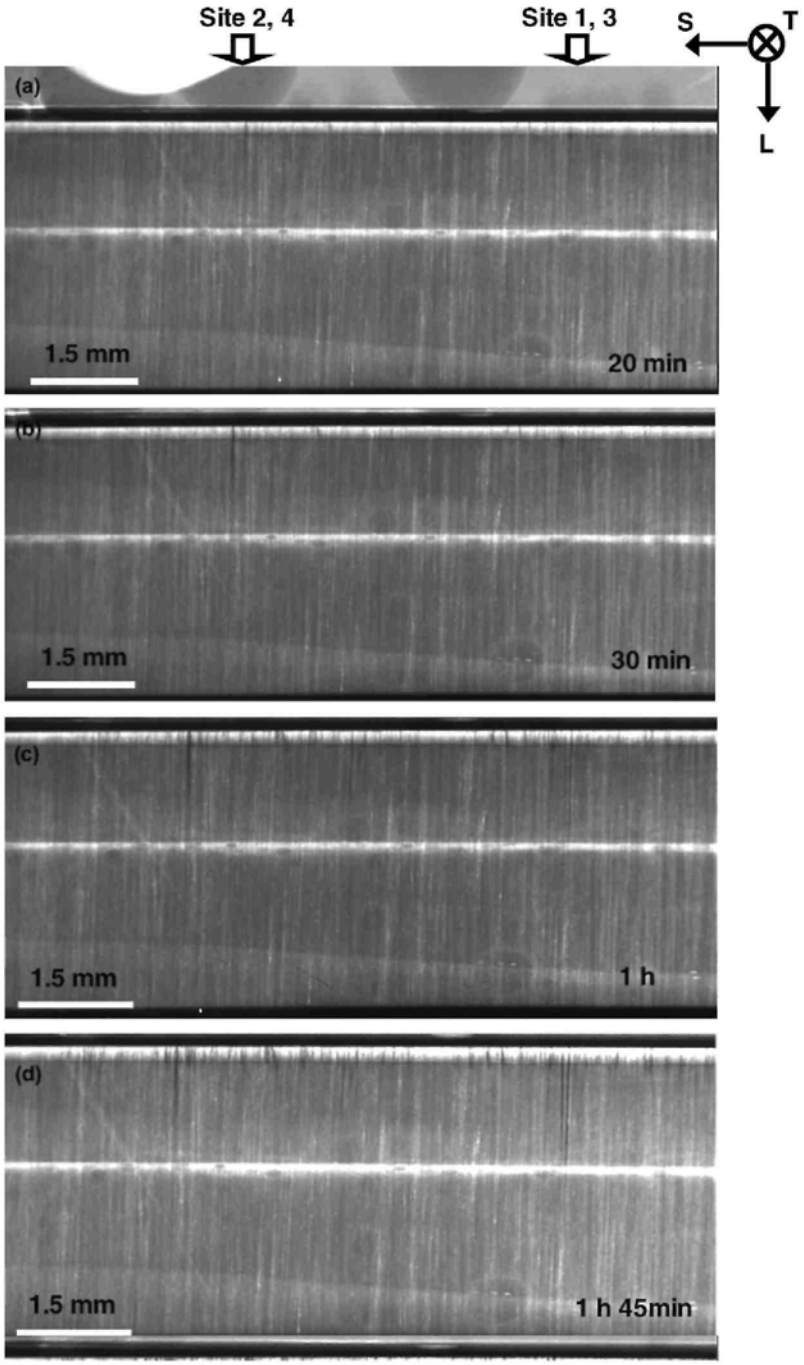

Fig. 2. Radiographic images of sample under constant load with initial stress of 77 MPa at —580 mV SCE in 1 M NaCl for 7 h: (a) at 20 min; (b) at 30 min; (c) at 1 h; (d) at 1 h 45 min; (e) at 3 h; (f) at 6.5 h; (g) at 7 h; and (h) after the sample broke at time of 7 h 4 min.

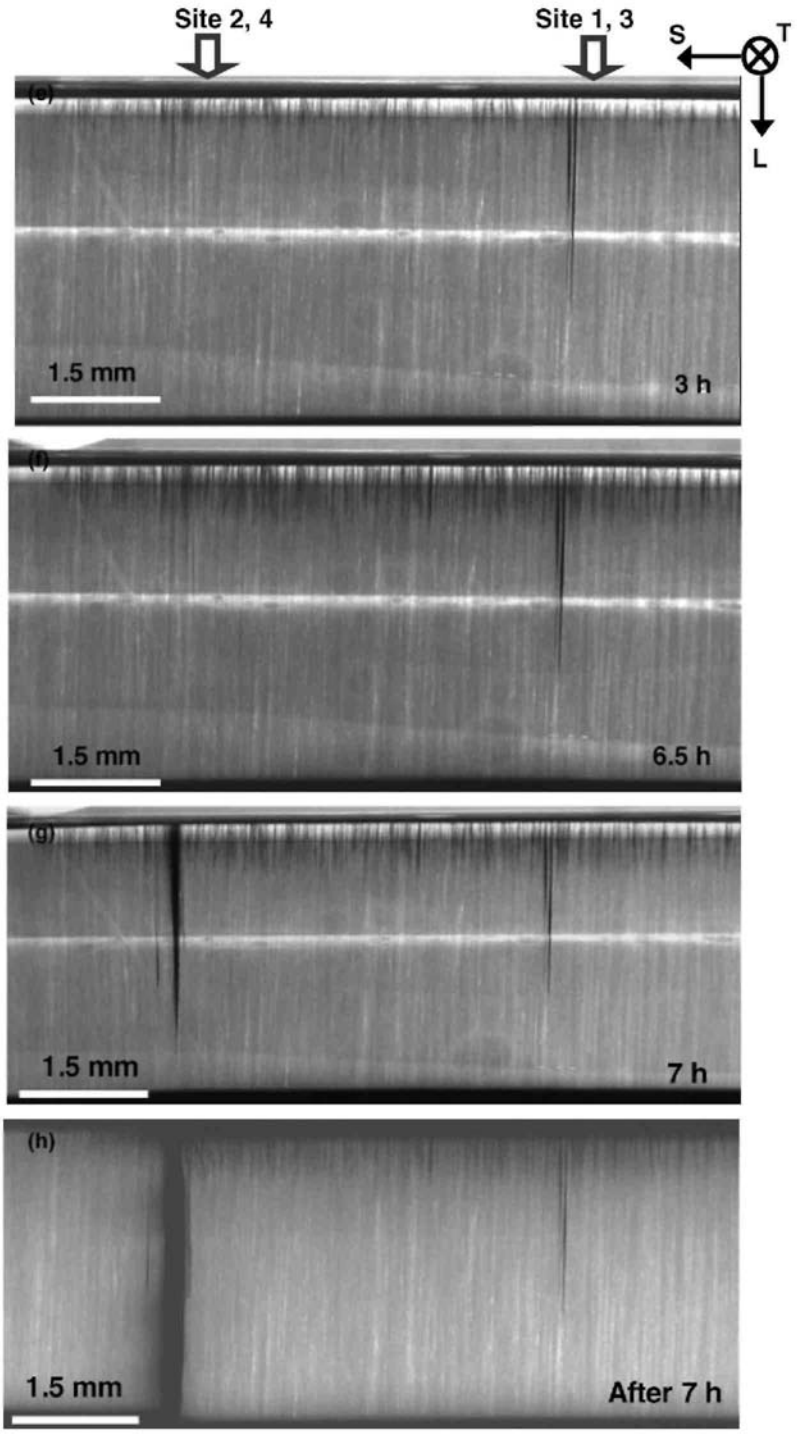

Fig. 2 (continued)

3.2. Analysis of IGSCC growth and quantification of stress intensity

Fig. 3 shows the length of the failure crack at site 4 as a function of time as well as the lengths of several stifled cracks, which are grouped in the shaded region. This figure shows clearly how the failure crack grew slowly during the test and then transitioned to a fast growth rate after 6 h.

Stress intensity (K) at the crack tip is the dominant driving force in mechanical fracture [21]. K for an array of equal-length and equal-spaced parallel cracks in a semi-infinite plate has been formulated [13,14], but the variable-spaced cracks of varying length in the current study are quite different. Therefore, the single edge notched tension (SENT) model was used to quantify K of the cracks [22]:

$$K = \frac{P}{B\sqrt{W}}\left[\frac{\sqrt{2\tan\frac{\pi a}{2W}}}{\cos\frac{\pi a}{2W}}\left(0.752 + 2.02\left(\frac{a}{W}\right) + 0.37\left(1 - \sin\frac{\pi a}{2W}\right)^3\right)\right] \quad (1)$$

where P is the constant load, B is the plate thickness (0.105 cm), W is the whole width of the sheet sample (0.375 cm), and a is the active crack length. The dimensions of this sample result in plane stress conditions. Fig. 4(a) shows the stress intensity calculated for the stifled crack at site 3 and the failure crack at site 4 as a function of time and Fig. 4(b) shows the da/dt vs. K curves. The growth rate of the stifled cracks slowed as they grew longer despite the increase in K. As a result, the da/dt–K curves for these cracks have very different shapes than what is typically found for growing cracks. This suggests that K is not the determining factor in crack growth for these stress corrosion cracks. The local susceptibility to intergranular stress corrosion appears to be a significant factor.

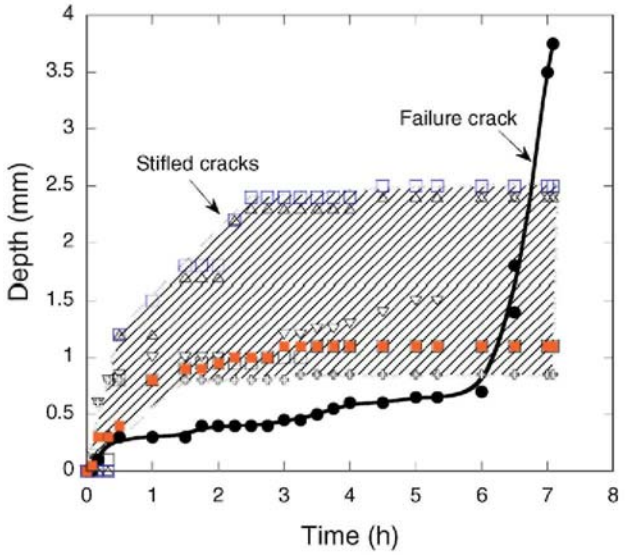

Fig. 3. IGSCC depth as a function of time for sample with initial stress of 77 MPa at —580 mV SCE in 1 M NaCl for 7 h.

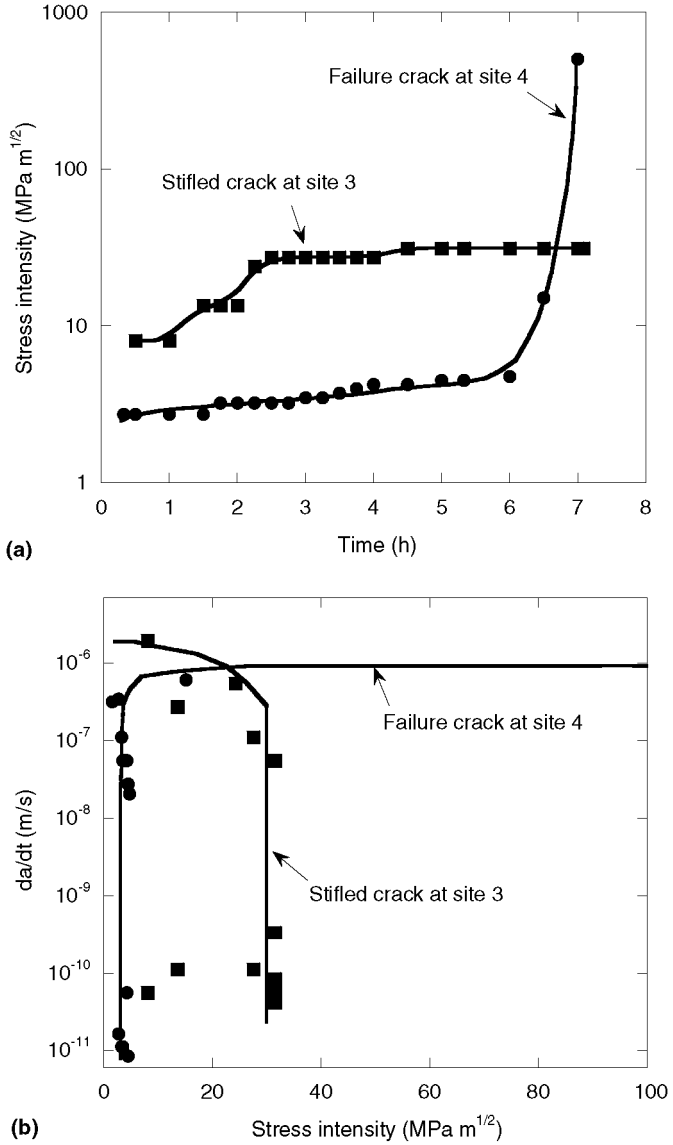

Fig. 4. Variation in stress intensity and IGSCC growth rate for the sample with initial stress of 77 MPa. (a) stress intensity as a function of time and (b) crack growth rate with variation of stress intensity.

4. Discussion

In this study, X-ray radiography was used to monitor the growth and competition of multiple IGSCCs. The condition of constant load results in an increasing stress intensity for growing cracks. According to the theory of fracture mechanics, the longest crack should have the highest stress intensity and grow preferentially to the other shallow cracks. However, in this study and other unreported tests [18] the crack that resulted in ultimate failure was not the longest crack at the early stages, whereas long cracks tended to stop growing. This phenomenon was not observed in the absence of applied stress, where IGC grew uniformly across the sample at a uniform rate [17]. The slowing and acceleration of different cracks in a single sample only was observed for stressed samples in a constant displacement jig [15-17] or in the constant load setup.

The plane strain fracture toughness (K_{IC}) can be determined using different types of specimens and methods. K_{IC} values reported for wrought AA2024-T351 single-edge notched plate less than one inch thick are in the range of 28-51 MPa $m^{1/2}$, depending on the microstructure [23]. Besides the factors of cracking orientation and metallurgy, the critical stress intensity factor for SCC, K_{ISCC}, is also dependent upon environment. A study of DCB specimens with crack-stress orientation similar to the specimen in this work reported K_{ISCC} = 8 MPa $m^{1/2}$ and 2nd stage cracking rate $da/dt = 7 \times 10^{-9}$ m/sec for AA2024-T351 at open circuit potential in 3.5% NaCl at 23 °C [24].

Even though the current test specimens were thin and short-width plates in the plane stress condition and contained multiple cracks, the K values are comparable to the published data. As shown in Fig. 4(a), the initial longer crack at site 3 was observed at the value of K= 8 MPa $m^{1/2}$ after 20 min, which is similar to K_{ISCC} for a thick plane strain specimen [24]. This suggests that the initial growth of the crack was at the critical condition for SCC crack stability, or K_{ISCC}. K for this crack increased with crack growth, but then leveled off as it stifled at K = 30 MPa $m^{1/2}$. The crack at site 4 started growing at $K = 2$ MPa $m^{1/2}$ during the first 20 min and K then increased slowly over 6 h as the crack grew slowly. During this time, it can be considered that this crack was IGC and not IGSCC, which explains the crack growth at low K values. However, after 6 h, the crack at site 4 started growing faster, which is likely associated with the transition from IGC to IGSCC. Interestingly, at this transition point, the K value is just above 8 MPa $m^{1/2}$, supporting the notion of K_{ISCC} = 8 MPa $m^{1/2}$. This crack then grew quickly and failed the sample. The da/dt-K plot in Fig. 4(b) shows the cracking rate at the 2nd stage was around 1×10^{-6} m/sec, which is about 100 times higher than reported values from standard DCB tests [24]. This difference probably resulted from the high potential applied to the sample; the reported values were at OCP.

The stifling of long cracks and acceleration of shorter cracks indicate that the effects of electrochemistry and local susceptibility of the microstructure are significant or even dominant in the crack growth process. The strong effect of electrochemistry might result from the applied potential (—580 mV SCE), which is relatively high and strongly promoted the formation of localized corrosion in the form of IGC. Controlled by a potentiostat, the available current was essentially infinite. So the stifling of cracks did not result from current limitations. Shortly after IGC initiated and started growing, one of the sites became an active SCC site and grew faster. IGC continued at a slower rate at the other sites as the SCC crack propagated. Therefore, there was no chance for different cracks to be competing for a fixed cathodic current, which can occur under open circuit conditions.

For linear elastic fracture mechanics to be valid, the small scale yield (SSY) criterion must be upheld to avoid surface effects. SSY requires the active crack length, a, and the remaining amount of sample in the cracking direction, $b = (W - a)$, to be larger than $2.5(K/\sigma_{ys})^2$, where σ_{ys} is yield stress [22]. In these experiments, the sample width, W, is 3.8 mm. Assuming crack growth at the critical condition of $K = K_{ISCC}$, the critical dimension is 1.3 mm. Therefore, the region of crack growth where the SSY criterion is upheld is limited in the samples used in this work. The initial long crack stopped growing at a dimension close to where the SSY criterion was invalid, so it is possible that the crack stifling was a result of the yield zone ahead of the crack changing as a result of the sample configuration, i.e., the limited remaining uncracked material can result in large scale yielding that might blunt the crack tip. However, this explanation does not account for the acceleration of a shorter crack that ultimately propagates through the sample.

It is also possible that the stifling of cracks occurs when they intersect triple points where one grain ends. The initial crack stifled at around 2 mm length, which is similar to the grain dimension in the L direction. At such an intersection, the conditions at the crack tip might change. One possibility is that the direction of the grain boundary changes at the triple point intersection so that the resolved stress at the crack tip is decreased. However, the very high aspect ratio of the grains in this material suggests that geometric effects on stress and stress intensity should be minimal.

The local GB composition could also change from one grain to another so that the stifling may take place when the IGC reaches a GB with an altered composition (including GB precipitates and neighboring precipitate free zone) that is much more resistant to SCC. The rapid acceleration of other cracks might be caused by a crack moving to a GB that is more susceptible to SCC. No definitive evidence supporting a mechanism for crack stifling was generated in this work.

5. Conclusions

Intergranular stress corrosion cracks in AA2024-T3 were characterized using a constant load setup that allowed multiple cracks to grow and compete with following observations:

1. In every experiment, the longest crack at early stages stopped growing and was passed by a crack at another site.
2. Stress intensity can be used to characterize the contribution of mechanical driving force in IGSCC, but it appears not to be the dominant driving force for cracking in a corrosive environment.
3. The effects of electrochemistry and local susceptibility of the microstructure play significant roles in IGSCC propagation.
4. The transition of IGC to IGSCC has been identified with a stress intensity equal to the critical stress intensity factor for stress corrosion cracking, K_{ISCC}.

Acknowledgements

This work was supported by the US Air Force Office of Scientific Research through Grant No. F49620-02-1-0148. The contract monitors were Lt. Col. Paul Trulove, PhD,and Major Jennifer Gresham, PhD. The authors especially thank Ken Kushner for fabricating the constant load frame.

References

[1] M.O. Speidel, Metallurgical and Materials Transactions A 6A (1975) 631–651.
[2] H. Vogt, M.O. Speidel, Corrosion Science 40 (1998) 251–270.
[3] R.H. Jones, R.E. Ricker (Eds.), Mechanisms of Stress–Corrosion CrackingR.H. Jones (Ed.), Stress–Corrosion Cracking Materials Performance and Evaluation, ASM International, 1992, pp. 1–20.
[4] M. Ahmad, Materials Science and Engineering A125 (1990) 1–14.
[5] T.D. Burleigh, Corrosion 47 (1991) 89–98.
[6] N.J.H. Holroyd, in: EICM Proceedings,1990, p. 311–345.
[7] W.J.D. Shaw, M.A. Fraser, T.S. Nijar, Microstructure Science 26 (1998) 269–276.
[8] R.P. Wei, C.-M. Liao, M. Gao, Metallurgical and Materials Transactions A 29A (1998) 1153–1160.
[9] R.G. Buchheit, M.A. Martinez, L.P. Montes, Journal of Electrochemical Society 147 (2000) 119–124.
[10] T. Ramgopal, P.I. Gouma, G.S. Frankel, Corrosion 58 (2002) 687–697.
[11] P.V. Petroyiannis, E. Kamoutsi, Al.Th. Kermanidis, S.G. Pantelakis, V. Bontozoglou, G.N. Haidemenop-oulos, Fatigue Fracture Engineering Material Structure 28 (2005) 565–574.
[12] S.P. Lynch, Acta Materialia 36 (1988) 2639–2661.

[13] T. Fett, D. Munz, Stress Instensity Factors and Weight Functions, Computational Mechanics Publications, Southampton UK and Boston USA, 1997, pp. 265–269.
[14] H. Tada, P. Paris, G. Irwin, The Stress Analysis of Cracks Handbook, Paris Production, Inc, St. Louis, MO, 1985, pp. 247–252.
[15] Xiaodong Liu, G.S. Frankel, B. Zoofan, S.I. Rokhlin, in: D. Shifler, T. Tsuru (Eds.), Corrosion in Marine and Saltwater Environments II, The Electrochemical Society proceedings Series, PV 2005-14, Honolulu, HI, 2004, pp. 223–231.
[16] Xiaodong Liu, G.S. Frankel, B. Zoofan, S.I. Rokhlin, Corrosion 62 (2006) 109–120.
[17] Xiaodong Liu, G.S. Frankel, B. Zoofan, S.I. Rokhlin, Journal of Electrochemical Society 153 (2006) B42–B51.
[18] Xiaodong Liu, in: Ph D thesis, The Ohio State University, 2005.
[19] Xiaodong Liu, G.S. Frankel, B. Zoofan, S.I. Rokhlin, Corrosion Science 46 (2004) 405–425.
[20] B. Zoofan, S.I. Rokhlin, Materials Evaluation 52 (1998) 191–194.
[21] ASTME1820-01, 2001, pp. 1025–1070.
[22] T.L. Anderson, Fracture Mechanics: Fundamentals and Applications, second ed., CRC press, 1995, pp. 62–90.
[23] J.G. Kaufman, in: Fracture Resistance of Aluminum Alloys: Notch Toughness, Teal Resistance, and Fracture ToughnessThe Aluminum Association, ASM International, Materials Park, OH, 2001, pp. 97–153.
[24] R.J. Bucci, G. Nordmark, J.E.A. Starke, in: Selecting Aluminum Alloys to Resist Failure by Fracture Mechanisms, Fatigure and FractureASM Handbook, vol. 19, ASM International, 1996, pp. 771– 812.